MNRAS Advance Access published May 31, 2016

ExoMol line lists XV: A new hot line list for hydrogen peroxide

Ahmed F. Al-Refaie[1], Oleg L. Polyansky[1,2], Roman I. Ovsyannikov[2], Jonathan Tennyson[1] and Sergei N. Yurchenko[1],
[1] *Department of Physics and Astronomy, University College London, Gower Street, WC1E 6BT London, UK*
[2] *Institute of Applied Physics, Russian Academy of Sciences, Ulyanov Street 46, Nizhny Novgorod, Russia 603950*

Accepted XXXX. Received XXXX; in original form XXXX

ABSTRACT

A computed line list for hydrogen peroxide, $H_2{}^{16}O_2$, applicable to temperatures up to $T = 1250$ K is presented. A semi-empirical high accuracy potential energy surface is constructed and used with an *ab initio* dipole moment surface as input TROVE to compute 7.5 million rotational-vibrational states and around 20 billion transitions with associated Einstein-A coefficients for rotational excitations up to $J = 85$. The resulting APTY line list is complete for wavenumbers below 6 000 cm^{-1} ($\lambda < 1.67$ μm) and temperatures up to 1250 K. Room-temperature spectra are compared with laboratory measurements and data currently available in the HITRAN database and literature. Our rms with line positions from the literature is 0.152 cm^{-1} and our absolute intensities agree better than 10%. The full line list is available from the CDS database as well as at `www.exomol.com`.

Key words: molecular data; opacity; astronomical data bases: miscellaneous; planets and satellites: atmospheres

1 INTRODUCTION

Terrestrial hydrogen peroxide exists as a trace molecule in the Earth's atmosphere and contributes to the atmospheres oxidising budget as well as ozone production and water chemistry (Davis 1974; Chance et al. 1991; Allen et al. 2013; Zins & Krim 2014) and its concentration is now being routinely observed (Allen et al. 2013). Astrophysically there have been multiple detections of H_2O_2 in the atmosphere of Mars (Clancy et al. 2004; Encrenaz et al. 2004, 2012; Aoki et al. 2015) with seasonal variation, possibly formed by triboelectricity in dust devils and dust storms (Encrenaz et al. 2012) and may well act as an agent in the oxidization of the Martian surface. Hydrogen peroxide has also been detected in the atmosphere of Europa (Hand & Brown 2013) in the 3.5 μm region. The first detection of interstellar H_2O_2 was made by Bergman et al. (2011) and is believed to play an important role in astrophysical water chemistry similar to that on Earth. Du et al. (2012) suggest that H_2O_2 is produced on dust-grains via the hydrogenation of grain HO_2 and released into the gas-phase through surface reactions. On the dust-grain, H_2O_2 acts as an intermediate in the formation of water and aids in the production of other species such as H_2CO, CH_3OH, and O_2.

Hydrogen peroxide belongs to the peroxide group of molecules with an HO-OH bond dissociation enthalpy of 17050 cm^{-1}(Bach et al. 1996) at 0 K. H_2O_2 is an asymmetric prolate rotor molecule and is the simplest molecule that exhibits internal rotation. This torsional motion gives rise to a double minimum potential curve with respect to its internal rotation co-ordinates as well as two alignments of the O-H bonds: *cis* and *trans*. The consequence of this motion means that there are four sub-levels for each torsional excitation which are characterized by their symmetry. This necessitates the use of an additional quantum number, τ, to unambiguously describe its motion. The molecular states can be classified using the C_{2h}^{+}(M) symmetry group which best describes the torsional splitting caused by the *cis* and *trans* tunneling (Hougen 1984). H_2O_2 has six vibrational modes: ν_1 and ν_5 represent the symmetric and asymmetric O-H stretching respectively, ν_3 and ν_6 represent the O-H bending modes, ν_2 represents the O-O stretch and the ν_4 mode represents the torsional excitation with the more common notation of n.

Experimental studies of ro-vibrational H_2O_2 spectra have mostly probed the torsional motion in the ground (Olson et al. 1988), the ν_3 (Camy-Peyret et al. 1992) and ν_6 (Perrin et al. 1990, 1995) vibrational modes. Conversely, the higher-lying O-H

stretching modes, ν_1 and ν_5, are poorly studied using high resolution techniques. The difference between the two stretching bands is about 8 – 10 cm^{-1} and torsional splitting from the double minimum of the potential gives rise to doubling (Giguere & Srinivasan 1974) in the form of 'quasi'-degenerate states (Rauhut et al. 2009) that are difficult to resolve with a degree of accuracy. Olson et al. (1988) give an estimate of 3610 - 3618 cm^{-1} for ν_5 and 3601 - 3617 cm^{-1} for ν_1 whilst a Raman study gives a lower value of 3607 cm^{-1} for the ν_1 band-centre (Giguere & Srinivasan 1974) but determining the accuracy to better than 0.1 cm^{-1} is difficult.

H_2O_2 has been a benchmark system for developing methods aiming to treat large amplitude motion (Luckhaus 2000; Mladenovic 2002; Yu & Muckerman 2002; Carter et al. 2009). Recent calculations on the ro-vibrational states for H_2O_2 include the *ab initio* computation using CCSD(T)-F12 electronic structure calculations of band frequencies accurate to about 4.0 cm^{-1} by Rauhut et al. (2009), models of the peroxide stretches by Bacelo & Binning (2005), a discrete variable representation (DVR) calculation for levels up to 6000 cm^{-1} by Chen et al. (2001); Lin & Guo (2003) and finally, a potential energy surface (PES) calculations by Koput et al. (1998) and Kuhn et al. (1999). Calculation which also consider transition intensities are rather rarer but a recent example is provided by Carter et al. (2011). The peroxide system was used to benchmark the large amplitude calculations of MULTIMODE (Bowman et al. 2003) up to $J = 20$ and showed good agreement against HITRAN line intensities but the PES used had an rms of ≈ 20 cm^{-1} against experimental band centers. However, this PES has been superceded by the higher accuracy *ab initio* potential energy surface (PES) of Małyszek & Koput (2013) which was further modified by Polyansky et al. (2013). This modified PES was used for our room-temperature line list (Al-Refaie et al. 2015a) and provides the starting point for the refinements performed here.

Experimental transitions frequencies and intensities for H_2O_2 are available in the HITRAN 2012 database (Rothman et al. 2013) but only for room temperature modelling up to 1800 cm^{-1}. This region covers the torsional, O-H bending modes and O-O stretch but misses the O-H stretches in the 3750 cm^{-1} region. Only a few studies deal with absolute intensities of H_2O_2 in the far-infrared (Zumwalt & Giguere 1941; Perrin et al. 1996, 1995) with only PNNL-IR (Sharpe et al. 2004) data providing integrated intensities in the mid-infrared region (Johnson et al. 2009). The thermal decomposition of hydrogen peroxide at 423 K makes it difficult and dangerous to study at higher temperatures.

Theoretical line lists can be used to fill in gaps in the experimental data both in terms of wavelength and temperature coverage. The ExoMol project (Tennyson & Yurchenko 2012) aims to produce comprehensive theoretical molecular line lists to aid in studies of the atmospheres of exoplanets, cool stars and other (hot) bodies. A room temperature line list for H_2O_2 was previously computed by us (Al-Refaie et al. 2015a) using the PES of Polyansky et al. (2013) and a new *ab initio* dipole moment surface (DMS). It provides about 1 billion transitions at up to 8,000 cm^{-1}. However it is limited as the rotational excitation of $J = 40$ makes it inadequate for high temperature modelling and the lower energy cut-off means that coverage above 4,000 cm^{-1} rapidly becomes incomplete. This work aims to build upon this line list by refining the PES towards spectroscopic accuracy and extending the temperature and frequency range for which the resulting line list is applicable.

2 METHOD

2.1 Potential energy Surface Refinement

Our previous room-temperature H_2O_2 line list (Al-Refaie et al. 2015a) was computed using the *ab initio* PES of Małyszek & Koput (2013) with the small adjustment of the *ab initio* equilibrium geometry and height of the torsional barrier proposed by Polyansky et al. (2013). This PES reproduces the known empirical energy levels with a root mean square (rms) of about 1–2 cm^{-1}. However, by utilising empirical band-centre shifting (Yurchenko et al. 2009) during the computation of the Hamiltonian, this was significantly reduced it to 0.001 – 0.1 cm^{-1} in the room temperature line list. The empirical shifting can be thought of as an addition to the *ab initio* PES producing an 'ad-hoc' PES which we will refer to as 'H2O2-2015' in comparisons below. Whilst band-centre shifting can reproduce experimental energies simply, its accuracy and predictive ability is limited to vibrational bands whose band centre positions are already experimentally characterised. A more robust method of correcting the PES is through fitting or refining to experimental energies. The TROVE nuclear motion program used by us here, see below, provides PES refinement capabilities and has been successful in producing accurate PES for molecules such as H_2CO (Yachmenev et al. 2011), NH_3 (Yurchenko et al. 2011a), SO_3 Underwood et al. (2014), PH_3 (Sousa-Silva et al. 2015) and CH_4(Yurchenko & Tennyson 2014).

The procedure implemented in TROVE describes a correction surface ΔV to the initial (*ab initio*) surface V. The new refined surface V' can therefore be written as $V' = V + \Delta V$ and the new Hamiltonian as $H' = H + \Delta V$, where H is the Hamiltonian if the starting point for the refinement. The wavefunctions from H, are used as basis-functions for H'. ΔV is expanded in Taylor series and the expansion coefficients, Δf_{ijklmn}, are obtained in a variational least-squares fit to spectroscopic data via the objective function F:

$$F = \sum_i^N w_i (E_i^{obs} - E_i)^2 = 0, \quad (1)$$

Table 1. Comparison of N weighted experimental data-points in the fit and non-weighted root mean squared deviation of both H2O2-2016 (this work) and H2O2-2015 (Al-Refaie et al. 2015a) for each dataset.

Weight	N	H2O2-2016 rms (cm^{-1})	H202-2015 rms (cm^{-1})	Comment
100	43	0.001	0.000	$J > 0$ pure torsional states
10-20	144	0.004	0.007	Band centers and $\nu_3 + \nu_4$, $\nu_6 + \nu_4$ states
1-9	186	0.539	1.369	Upper state extracted from HITRAN with corroborated lower states

Table 2. Comparision of N experimental data-points in the fit and weighted root mean squared deviation of both H2O2-2016 (this work) and H2O2-2015 (Al-Refaie et al. 2015a).

J	N	H2O2-2016 wrms (cm^{-1})	H202-2015 wrms (cm^{-1})
0	34	0.238	0.254
1	47	0.079	0.320
2	81	0.096	0.345
3	116	0.183	0.404
4	132	0.154	0.287
Total		0.150	0.321

where N is the number of observed energies E_i^{obs}, E_i are the calculated energies and w_i are the weights.

Here the original 282 expansion coefficients of the *ab initio* PES are reduced to 163 by removing the symmetry-related O-H stretching (ij) and bending (kl) terms from the input PES and simply linking them in the computation of potential energy terms in the Hamiltonian. This ensures that the symmetry of these terms is preserved during the fitting process. The quality of the fit is determined by the quality and vibrational diversity of the input dataset. Two sources of experimental data come from line-positions provided in the literature and transitions from HITRAN. The HITRAN dataset sources come from observations by Perrin et al. (1995), Perrin et al. (1996), Perrin et al. (1990) and Klee et al. (1999) with literature line-positions from Flaud et al. (1989), Olson et al. (1988) Giguere (1950), Zumwalt & Giguere (1941) and Camy-Peyret et al. (1992). This empirical dataset provides the ν_4, $\nu_3 + \nu_4$, $\nu_4 + \nu_6$ and ν_2 vibrational terms. Unfortunately there is little to no reliable data on the ν_1 and ν_5 energy levels, their reported band-centre values vary significantly in literature making them unsuitable for the refinement. This hampers the vibrational diversity that would aid in construction of an extensive fitted PES. However, these terms can be indirectly improved by including higher J values from other vibrational states.

Our input dataset includes all energies for $J \leqslant 4$ up to 4000 cm^{-1}. The weights w_i used have an arbitrary range of values that are normalized in the fit. The energies given in literature are the simplest to include in the refinement process and are given the highest weighting. Here the pure torsional band at $J > 0$ from Camy-Peyret et al. (1992) and Olson et al. (1988) are given the highest weighting of $w_i = 100$. The ν_2, ν_3, ν_6, $\nu_3 + \nu_4$, $\nu_4 + \nu_6$ energies and H_2O_2 band centers (except for ν_1 and ν_5) from Camy-Peyret et al. (1992), Giguere (1950), Perrin et al. (1990), Flaud et al. (1989) and Zumwalt & Giguere (1941) are given weights $10 \leqslant w_i \leqslant 20$.

Transitions from HITRAN require additional work. In order to determine the upper state of a transition requires the assignment of the lower state energy. Fortunately HITRAN provides the lower state energy for all transitions in the database. However, lower state energies require corroboration from literature data and/or the *ab initio* energies for the upper state energies to be included in the fit with $1 \leqslant w_i \leqslant 9$ based on confidence of the datum. Each input datum must be correlated with a theoretically computed energy level which, in this present work, was straightforward due to the good agreement given by the initial *ab initio* PES.

Special measures must be taken in order to ensure that the refinement process does not lead to unphysical shapes for the new PES due to a limited sampling of the experimental data not covering all the complexity of the potential energy surface of HOOH. For example the high stretching or bending overtones are poorly represented in the experimental and therefore it is important to retain the *ab initio* quality of the original PES by Polyansky et al. (2013). To this end we constrain the PES around *ab initio* energies at each geometry (Yurchenko et al. 2003, 2011b; Yachmenev et al. 2011; Sousa-Silva et al. 2015).

The new potential energy surface is called H2O2-2016. Table 1 describes the rms for states of a particular weight. The high quality of the H2O2-2016 energies computed without any empirical band shifts shows that this new semi-empirical PES performs better overall than the *ab initio* band-shifted PES especially for the lower weighted states. Weights $\geqslant$10 relate to vibrational states that were involved in the band-shifting which gives H2O2-2015 its low rms values. Comparing weights lower than 10 suggests that the predictive ability of the H2O2-2016 PES is greatly enhanced. The overall comparison as a function of the rotational quantum number J with a weighted rms is given in Table 2.

Overall H2O2-2016 improves the rms deviations of H2O2-2015 by more than a factor of 2. Table 3 highlights residuals for $J \geqslant 30$ for the ν_3 and ν_6 line positions from Camy-Peyret et al. (1992) and Perrin et al. (1990) and shows excellent agreement with an overall rms of 0.064 cm^{-1}. The rms deviation for all 2734 states in HITRAN up to $J = 49$ and energy up to 3461.02 cm^{-1}

Table 3. Residuals in cm^{-1} for energies computed from the H2O2-2016 PES. Observed data is from Camy-Peyret et al. (1992) and Perrin et al. (1990). The overall rms is 0.0642 cm^{-1}

J	K	ν_3	n	τ	ν_6	Obs	Calc	O-C	J	K	ν_3	n	τ	ν_6	Obs	Calc	O-C
30	0	0	0	1	0	789.58	789.64	-0.06	31	11	0	0	2	0	1950.60	1950.55	0.05
30	1	0	0	2	0	793.05	793.12	-0.07	31	11	0	0	3	0	1963.12	1963.07	0.05
30	2	0	0	1	0	829.29	829.34	-0.05	31	5	0	1	2	1	2577.85	2577.91	-0.06
30	2	0	0	4	0	841.34	841.32	0.02	31	1	0	2	2	1	2694.38	2694.48	-0.10
30	3	0	0	2	0	876.03	876.07	-0.04	31	2	0	2	1	1	2729.02	2729.07	-0.05
30	3	0	0	2	0	876.03	876.07	-0.04	31	3	0	2	2	1	2775.74	2775.66	0.08
30	4	0	0	1	0	940.03	940.07	-0.04	31	9	0	0	3	1	2877.92	2877.84	0.08
30	6	0	0	4	0	1134.61	1134.58	0.03	31	7	0	1	3	1	2940.33	2940.25	0.08
30	2	0	1	4	0	1198.50	1198.58	-0.08	31	9	0	1	3	1	3232.19	3232.21	-0.02
30	7	0	0	2	0	1241.30	1241.33	-0.03	32	1	0	0	2	0	898.70	898.78	-0.08
30	7	0	0	2	0	1241.30	1241.33	-0.03	32	2	0	0	1	0	936.15	936.21	-0.06
30	7	0	0	3	0	1253.29	1253.25	0.04	32	2	0	0	4	0	948.32	948.29	0.02
30	4	0	1	4	0	1308.34	1308.43	-0.09	32	3	0	0	2	0	983.10	983.16	-0.05
30	1	0	2	2	0	1362.75	1362.83	-0.08	32	4	0	0	1	0	1047.03	1047.07	-0.04
30	8	0	0	4	0	1390.06	1390.01	0.05	32	2	0	1	4	0	1305.21	1305.30	-0.09
30	5	0	1	3	0	1390.16	1390.27	-0.11	32	7	0	0	2	0	1347.93	1347.96	-0.03
30	2	0	2	1	0	1396.42	1396.52	-0.10	32	1	0	2	2	0	1468.52	1468.61	-0.09
30	9	0	0	3	0	1544.80	1544.75	0.05	32	8	0	0	4	0	1496.82	1496.77	0.05
30	0	1	0	1	0	1645.15	1645.20	-0.05	32	9	0	0	3	0	1651.43	1651.37	0.06
30	2	1	0	2	0	1688.11	1688.15	-0.03	32	0	1	0	1	0	1749.83	1749.89	-0.06
30	10	0	0	1	0	1707.36	1707.33	0.03	32	1	1	0	2	0	1752.86	1752.92	-0.07
30	10	0	0	4	0	1717.16	1717.10	0.06	32	2	1	0	1	0	1794.43	1794.46	-0.03
30	3	1	0	1	0	1731.55	1731.59	-0.04	32	10	0	0	4	0	1823.55	1823.48	0.07
30	11	0	0	2	0	1898.17	1898.11	0.06	32	3	1	0	2	0	1837.22	1837.26	-0.04
30	11	0	0	3	0	1910.47	1910.41	0.06	32	5	0	1	2	1	2631.92	2632.00	-0.08
30	6	1	0	2	0	1978.18	1978.19	0.00	32	9	0	0	3	1	2931.74	2931.70	0.04
30	5	0	1	2	1	2525.44	2525.50	-0.06	32	9	0	1	3	1	3285.71	3285.72	-0.01
30	0	0	2	1	1	2638.21	2638.21	0.00	33	4	0	0	1	0	1103.04	1103.09	-0.05
30	2	0	2	1	1	2678.98	2678.96	0.02	33	7	0	0	2	0	1403.73	1403.76	-0.03
30	6	0	1	4	1	2768.27	2768.35	-0.08	33	9	0	0	3	0	1707.24	1707.18	0.06
30	9	0	0	3	1	2825.75	2825.74	0.01	33	10	0	0	4	0	1879.23	1879.16	0.07
30	9	0	1	3	1	3180.32	3180.35	-0.03	33	5	0	1	2	1	2687.68	2687.77	-0.09
30	11	0	0	3	1	3196.72	3196.74	-0.02	33	7	0	2	2	1	3252.13	3252.10	0.03
30	10	0	1	4	1	3355.50	3355.61	-0.11	33	9	0	1	3	1	3340.86	3340.86	0.00
31	3	0	0	2	0	928.92	928.97	-0.04	34	2	0	0	4	0	1061.96	1061.93	0.03
31	4	0	0	1	0	992.69	992.73	-0.04	34	3	0	0	2	0	1096.87	1096.93	-0.06
31	6	0	0	4	0	1187.24	1187.21	0.03	34	4	0	0	1	0	1160.72	1160.77	-0.05
31	1	0	1	3	0	1230.77	1230.86	-0.09	34	2	0	1	4	0	1418.58	1418.69	-0.11
31	2	0	1	4	0	1253.76	1253.86	-0.10	34	7	0	0	2	0	1461.18	1461.23	-0.05
31	7	0	0	2	0	1293.78	1293.81	-0.03	34	10	0	0	4	0	1936.55	1936.48	0.07
31	7	0	0	2	0	1293.78	1293.81	-0.03	34	7	0	2	2	0	2026.09	2026.08	0.01
31	0	0	2	1	0	1410.64	1410.73	-0.09	34	0	0	0	4	1	2287.94	2288.05	-0.11
31	0	0	2	1	0	1410.64	1410.73	-0.09	34	5	0	1	2	1	2745.11	2745.21	-0.10
31	8	0	0	4	0	1442.61	1442.56	0.05	34	9	0	1	3	1	3397.65	3397.63	0.02
31	9	0	0	3	0	1597.29	1597.23	0.06	35	1	0	0	2	0	1091.72	1091.77	-0.05
31	1	1	0	2	0	1717.38	1717.60	-0.23	35	4	0	0	1	0	1220.07	1220.13	-0.06
31	2	1	0	1	0	1736.75	1736.79	-0.05	35	7	0	0	2	0	1520.29	1520.34	-0.05
31	10	0	0	4	0	1769.53	1769.46	0.07	35	1	0	0	2	1	2324.23	2324.16	0.07
31	3	1	0	2	0	1783.76	1783.79	-0.03	35	1	0	0	2	1	2324.23	2324.16	0.07
31	4	1	0	1	0	1847.46	1847.49	-0.03	36	2	0	0	4	0	1182.24	1182.21	0.03

is 0.834 cm^{-1}. Vibrational terms that correspond to the highest weighted states have an rms of 0.192 cm^{-1}. Around 12 states related to higher excited torsional modes $n > 3$ have an rms of 5.2 cm^{-1} and may well be due to misassignments. This PES is therefore of there of improved accuracy and is the one used below. The coefficients defining this PES are given in the Supplementary Information.

2.2 Variational computation

Theoretical ROVibrational Energies (TROVE) (Yurchenko et al. 2007) was employed to compute the ro-vibrational energies of H_2O_2. TROVE is a variational nuclear motion solver and was used to successfully produce the room temperature H_2O_2

line list as well as hot line lists for NH_3 (Yurchenko et al. 2011a), CH_4 (Yurchenko & Tennyson 2014), PH_3 (Sousa-Silva et al. 2015), H_2CO (Al-Refaie et al. 2015b) and SO_3 (Underwood et al. 2016).

TROVE can operate with any co-ordinate system of our choosing by utilizing an approximate kinetic energy operator (KEO). For H_2O_2, this approximate KEO was shown by Polyansky et al. (2013) to produce results that are in very good agreement with the exact KEO code WAVR4 (Kozin et al. 2004). However, the computational cost is greatly reduced for rotationally excited states by using TROVE. Convergence of the KEO usually requires an expansion order of 6 or 8 (Yurchenko et al. 2007); 6 being chosen for this work and 8 for the potential energy expansion as suggested from a previous H_2O_2 calculation by Polyansky et al. (2013).

Basis sets and wave functions are symmetrized to the $\mathcal{D}_{2h}$(M) molecular symmetry group (Bunker & Jensen 1998) which is isomorphic to the C^+_{2h}(M) symmetry group. This has the benefit of factorizing the Hamiltonian into smaller independent blocks for diagonalization. The irreducible representations of this group are A_g, A_u, B_{1g}, B_{1u}, B_{2g}, B_{2u}, B_{3g} and B_{3u}. However, the states corresponding to B_{2g}, B_{2u}, B_{3g} and B_{3u} have zero nuclear statistical weight and therefore these matrix blocks are not needed for $J > 0$. The corresponding $J = 0$ energies from these representations are also unphysical, but computed and kept as vibrational band centres for reference purposes.

A symmetry-adapted basis-set is constructed by a multi-step contraction scheme by solving the 1D Schrödinger equation via the Numerov-Cooley method (Noumerov 1924; Cooley 1961) for the basis-functions $\phi_{n_i}(\zeta_i)(i = 1, 2, ..., 6)$, where ζ_1 represents the O-O stretching co-ordinate, ζ_2) and ζ_3 represent the O-H stretching co-ordinates, ζ_4 and ζ_5 represents the O-H bending modes and ζ_6 represents the torsional mode. n_i is the local mode quantum number assigned by TROVE. The basis functions ϕ_{n_i} are then used to form a product-type basis set, which is truncated by the polyad number P:

$$P = 4n_1 + 8(n_2 + n_3 + n_4 + n_5) + n_6 \leqslant P_{\max}. \tag{2}$$

We use $P_{\max} = 42$ as it was found to give good convergence (Polyansky et al. 2013). The second step requires computing a contracted basis set by reducing the six dimensional co-ordinates into four dimensions. This accomplished by reducing the 6-dimensional co-ordinate system into four subspaces: (ζ_1), (ζ_2, ζ_3), (ζ_4, ζ_5) and (ζ_6) based on their permutation properties. The reduced Hamiltonian is solved using the primitives ϕ_{n_i} as basis functions to obtain the symmetrised vibrational eigenfunctions $\Phi_{\lambda_1}(\zeta_1)$, $\Phi_{\lambda_2}(\zeta_2, \zeta_3)$, $\Phi_{\lambda_3}(\zeta_4, \zeta_5)$ and $\Phi_{\lambda_4}(\zeta_6)$. The vibrational contracted basis set is then formed from symmetrized products of these eigenfunctions which is also truncated via Eq. (2). A final contraction step is performed by solving the $J = 0$ problem and replacing the bulky primitive and contracted vibrational basis set with the more compact $J = 0$ wavefunctions $\Psi_i^{J=0,\Gamma}$ truncated at 12 000 cm^{-1}. The benefit of this is that the computation of the Hamiltonian matrix elements for $J > 0$ is more efficient and reduces the size of the matrix. Whilst this form means we can replace the diagonal vibrational terms with experimental band centers, the low rms error of H2O2-2016 PES band centers makes this procedure unnecessary. Our final ro-vibrational wavefunction has the form:

$$\Psi^{J,\Gamma} = \sum_{i,K,p} c_{i,K,p} \Psi_i^{J=0,\Gamma} |J, K, p\rangle, \tag{3}$$

where $|J, K, p\rangle$ are rigid rotor functions with parity p defined by Yurchenko et al. (2005a) and $c_{i,K,p}$ are the eigenvector coefficients obtained by diagonalization of the Hamiltonian matrix. The linear algebra libraries LAPACK (Anderson et al. 1999) and SCALAPACK (Blackford et al. 1997) were employed to solve for the eigenvalues and eigenvectors.

TROVE assigns six local mode n_i quantum numbers to each state by finding the largest contributing $c_{i,K,p}$. These can be reassigned to match the more standard normal modes v_i generally used in literature. However, TROVE only provides six quantum numbers for reassignment, when seven are required by the inclusion of τ. The τ quantum number can be preserved in the reassignment in TROVE by utilizing the following form:

$$v_4 = 4n + i, \tag{4}$$

where n is the excitation and i is the symmetry where $i = 0, 1, 2, 3$ is A_g, B_{2u}, B_{2g} and A_u respectively. To retrieve n and τ simply requires:

$$\tau = (v_4 \bmod 4) + 1, \quad n = \left\lfloor \frac{v_4}{4} \right\rfloor. \tag{5}$$

2.3 Dipole moment surface and intensities

An electric dipole moment surface (DMS) is required in order to compute transition intensities. The *ab initio* DMS of Al-Refaie et al. (2015a) was utilized; this was computed at the CCSD(T)-f12b (Bartlett & Musiał 2007) level of theory in the frozen-core approximation and is applicable to energies up to hc 12 000 cm^{-1}.

The eigenvectors, obtained by diagonalization, are used in conjunction with the DMS to compute the required linestrengths and Einstein-A coefficients of transitions that satisfy the rotational selection rules

$$J' - J'' = 0, \pm 1, J' + J'' \neq 0 \tag{6}$$

and the symmetry selection rules:

$$A_g \leftrightarrow A_u, B_{1g} \leftrightarrow B_{1u} \tag{7}$$

applied to para and ortho states, respectively. States with B_{2g}, B_{2u}, B_{3g} and B_{3u} symmetry are forbidden due their zero nuclear statistical weights.

The Einstein-A coefficient for a particular transition from the *initial* state i to the *final* state f is given by:

$$A_{if} = \frac{8\pi^4 \tilde{\nu}_{if}^3}{3h}(2J_i+1) \sum_{A=X,Y,Z} |\langle \Psi^f | \bar{\mu}_A | \Psi^i \rangle|^2, \tag{8}$$

where J_i is the rotational quantum number for the initial state, h is Planck's constant, $\tilde{\nu}_{if}$ is the transition frequency ($hc\,\tilde{\nu}_{if} = E_f - E_i$), Ψ^f and Ψ^i represent the eigenfunctions of the final and initial states respectively, $\bar{\mu}_A$ is the electronically averaged component of the dipole moment along the space-fixed axis $A = X, Y, Z$ (see also Yurchenko et al. (2005b)). From this the absolute absorption intensity is determined by:

$$I(f \leftarrow i) = \frac{A_{if}}{8\pi c} g_{\rm ns}(2J_f+1) \frac{\exp\left(-\frac{c_2 \tilde{E}_i}{T}\right)}{Q\ \tilde{\nu}_{if}^2} \left[1 - \exp\left(\frac{-c_2 \tilde{\nu}_{if}}{T}\right)\right],$$

where $c_2 = hc/k$ is the second radiation constant, $\tilde{E}_i$ is the energy term value, T the absolute temperature and $g_{\rm ns}$ is the nuclear spin statistical weight factor. Q, the partition function, is given by:

$$Q = \sum_i g_i \exp\left(\frac{-c_2 \tilde{E}_i}{T}\right), \tag{9}$$

where g_i is the degeneracy of a particular state i with the energy term value $\tilde{E}_i$. For H_2O_2, g_i is $g_{\rm ns}(2J_i+1)$ with $g_{\rm ns} = 1$ for A_g and A_u symmetries and $g_{\rm ns} = 3$ for B_{1g} and B_{1u} symmetries. The transitions were computed using the energy limits hc 6 000 and hc 12 000 cm^{-1} for the lower and upper states, respectively giving a complete coverage of the region 0 – 6 000 cm^{-1} ($\lambda > 1.67$ μm).

The intensities were computed using an enhanced version of TROVE that utilizes the nVidia graphics processing units (GPU) allowing for the computation of 5,000–30,000 transitions per second on a single GPU. The GPUs utilized were the nVidia M2090, K20 and the K40 models. A paper discussing this will be published elsewhere (Al-Refaie et al. 2016).

3 RESULTS

The final hot line list named APTY contains 7 560 352 states and almost 20 billion transitions that completely cover the 0 – 6 000 cm^{-1} region. An extended line list is provided which contains an additional 8 billion transitions in the 6 000– 8 000 cm^{-1} region with reduced completeness for higher temperature. Radiative lifetimes are also computed via the methodology presented by Tennyson et al. (2016a). Figure 1 presents the lifetimes computed for states up to 6 000 cm^{-1}. Here the complicated rotational structure of H_2O_2 gives rise to long lived lower state energies with lifetimes that can reach up to 30 million years. Extract from the ExoMol-form (Tennyson et al. 2013, 2016b) states and transition files are given in Tables 4 and 5. Spectra at arbitrary temperatures can be computed using the Einstein-A coefficients from the transition files.

An estimate of the temperature applicability of the line list can be performed by checking the partition function convergence of Eq. (9), which is computed via explicit summation (Vidler & Tennyson 2000). The convergence can be measured by computing $(Q_J - Q_{J-1})/Q_J$ where Q_J is the partition function for all energy levels up to rotational excitation J. For 296 K, the partition function converges to 0.001% at $J = 37$ which matches the room temperature line list's J limit of $J = 40$. At higher temperatures, it is well-converged up to at least 1500 K where the estimated error is only 0.2 % at $J = 85$. This can be attributed to the good coverage of J states computed that contribute to the overall population. A second partition Q_{lim} can be evaluated by only including states that fall below the hc 6 000 cm^{-1} lower state energy limit of the line list and compared against Q by computing the ratio Q_{lim}/Q to assess the completeness of the full line list. Figure 2 shows that at up to 800 K, the partition functions are essentially the same. At 1250 K about 90% of the population of states is represented by Q_{lim} but this falls to ≈80% at 1500 K giving the upper temperature for which APTY is reasonably complete as 1250 K. Usage of the line list at higher temperatures runs the risk of losing opacity due to missing contributions. The ratio Q_{lim}/Q can be used to estimate this. However, the decomposition of H_2O_2 means that it is unlikely to be an important species above 1000 K. The partition function tabulated in steps of 1 K, alongside an associated cooling function, is given as Supplementary Information to this article.

Table 6 compares our partition function against HITRAN; we see that at temperatures less than 1000 K we agree better than 1%. For temperatures 1000 – 1500 K, the APTY partition function is greater by 2–4% suggesting that the explicit summation method gives higher, and probably better values, than the more approximate method used by HITRAN (Fischer et al. 2003). However, at 3000 K APTY's Q is 30% lower than the HITRAN value which can be attributed to the eigenvalue

Table 4. Extract from the H_2O_2 state file. The full table is available at `http://cdsarc.u-strasbg.fr/cgi-bin/VizieR?-source=J/MNRAS/`.

I	$\tilde{E}$,cm^{-1}	g	J	L	$\Gamma_{\rm tot}$	v_1	v_2	v_3	v_4	v_5	v_6	τ	$\Gamma_{\rm vib}$	K	p	$\Gamma_{\rm rot}$	$I_{J,\Gamma}$	$\lvert C_i^2\rvert$	n_1	n_2	n_3	n_4	n_5	n_6
1	0.0	1	0	inf	1	0	0	0	0	0	0	1	1	0	0	1	1	0.95	0	0	0	0	0	0
2	254.54376	1	0	6.9464D-01	1	0	0	0	1	0	0	1	1	0	0	1	2	0.94	0	0	0	0	0	4
3	569.726553	1	0	3.1256D-01	1	0	0	0	2	0	0	1	1	0	0	1	3	0.94	0	0	0	0	0	8
4	865.942367	1	0	3.1317D+01	1	0	0	1	0	0	0	1	1	0	0	1	4	0.87	1	0	0	0	0	0
5	1000.872029	1	0	1.7264D-01	1	0	0	0	3	0	0	1	1	0	0	1	5	0.93	0	0	0	0	0	12
6	1119.712431	1	0	6.8795D-01	1	0	0	1	1	0	0	1	1	0	0	1	6	0.85	1	0	0	0	0	4
7	1391.868926	1	0	6.8101D+00	1	0	1	0	0	0	0	1	1	0	0	1	7	0.44	0	0	0	1	0	0
8	1432.296785	1	0	2.9134D-01	1	0	0	1	2	0	0	1	1	0	0	1	8	0.81	1	0	0	0	0	8
9	1477.148868	1	0	1.2710D-01	1	0	0	0	4	0	0	1	1	0	0	1	9	0.84	0	0	0	0	0	16
10	1679.479144	1	0	5.6793D-01	1	0	1	0	1	0	0	1	1	0	0	1	10	0.42	0	0	0	1	0	4
11	1714.839900	1	0	1.5294D+01	1	0	0	2	0	0	0	1	1	0	0	1	11	0.80	2	0	0	0	0	0
12	1862.945393	1	0	1.7244D-01	1	0	0	1	3	0	0	1	1	0	0	1	12	0.82	1	0	0	0	0	12
13	1945.069104	1	0	1.1596D-01	1	0	0	0	5	0	0	1	1	0	0	1	13	0.74	0	0	0	0	0	20
14	1967.624310	1	0	6.7322D-01	1	0	0	2	1	0	0	1	1	0	0	1	14	0.77	2	0	0	0	0	4
15	1973.269531	1	0	2.8904D-01	1	0	1	0	2	0	0	1	1	0	0	1	15	0.39	0	0	0	1	0	8
16	2240.375911	1	0	4.8422D+00	1	0	1	1	0	0	0	1	1	0	0	1	16	0.35	1	0	0	1	0	0
17	2280.037817	1	0	2.8806D-01	1	0	0	2	2	0	0	1	1	0	0	1	17	0.72	2	0	0	0	0	8

$\mathcal{D}_{2h}$(M) represention: 1 is A_g, 2 is A_u, 3 is B_{1g}, 4 is B_{1u}, 5 is B_{2g}, 6 is B_{2u}, 7 is B_{3g} and 8 is B_{3u}
I: State counting number;
$\tilde{E}$: State term energy in cm^{-1};
g: State degeneracy;
J: State rotational quantum number;
L: Lifetime (s)
$\Gamma_{\rm tot}$: Total symmetry in $\mathcal{D}_{2h}$(M) (A_g, A_u, B_{1g} and B_{1u} only)
v_1,v_2,v_3,v_5,v_6: Normal mode vibrational quantum numbers;
n: torsional mode excitation;
τ: torsional symmetry;
$\Gamma_{\rm vib}$: Symmetry of vibrational contribution in $\mathcal{D}_{2h}$(M);
K: State projection of the rotational quantum number;
p: Rotational parity;
$\Gamma_{\rm rot}$: Symmetry of rotational contribution in $\mathcal{D}_{2h}$(M);
$I_{J,\Gamma}$: State number in J,Γ block;
$|C_i^2|$: Largest coefficient used in the assignment;
$n_1 - n_6$: TROVE vibrational quantum numbers.

Table 5. Extracts from the H_2O_2 transitions file. The full table is available at `http://cdsarc.u-strasbg.fr/cgi-bin/VizieR?-source=J/MNRAS/`

f	i	A_{fi}
4893324	4865894	2.5558e-33
6064947	6004042	5.0185e-24
978337	813317	2.3963e-29
5920140	5983274	9.1885e-25
4838267	4920666	1.5740e-25
2328674	2173645	7.2614e-33

f: Upper state counting number;
i: Lower state counting number;
A_{fi}: Einstein-A coefficient in s^{-1}.

cutoff of 12 000 cm^{-1} and $J = 85$. Studies on ammonia and phosphine have shown that considerably extended lists of energy levels are required to get converged partition sums at these elevated temperatures (Sousa-Silva et al. 2014).

Figure 3 is a simulated spectrum of the APTY line list computed at $T = 296$ K. This highlights the coverage and sheer number and density of transitions available compared to the current edition of the HITRAN database (Rothman et al. 2013). Figure 4 compares our results with specific regions in the HITRAN database, the torsional and ν_6 bands. Comparisons of the two show excellent agreement in replicating both line position and intensities.

Our line list in the ν_1 and ν_5 band regions can be validated by simulating absorption cross sections in the the 2.7 μm region and comparing against PNNL-IR data (Sharpe et al. 2004). The structure and positions are in good agreement with the overall integrated intensity for APTY in this region being 3% stronger than PNNL. The improvement given by the H2O2-2016 PES can be demonstrated by comparing with our previous room temperature line list and with the PNNL-IR data; see Figure 6. The wavelengths of the largest two peaks in this band at 2.738 μm and 2.736 μm are correctly reproduced by APTY but are shifted by about 0.001 μm for H2O2-2015, showing the improvement in this band due to use of the refined PES. Overall the integrated cross-sections for this band differs only by 3% from PNNL; indeed the entire spectrum up to 6,000 cm^{-1} only differs by 3%.

Band intensities can be computed by explicit summation of all transitions within a band and compared against available

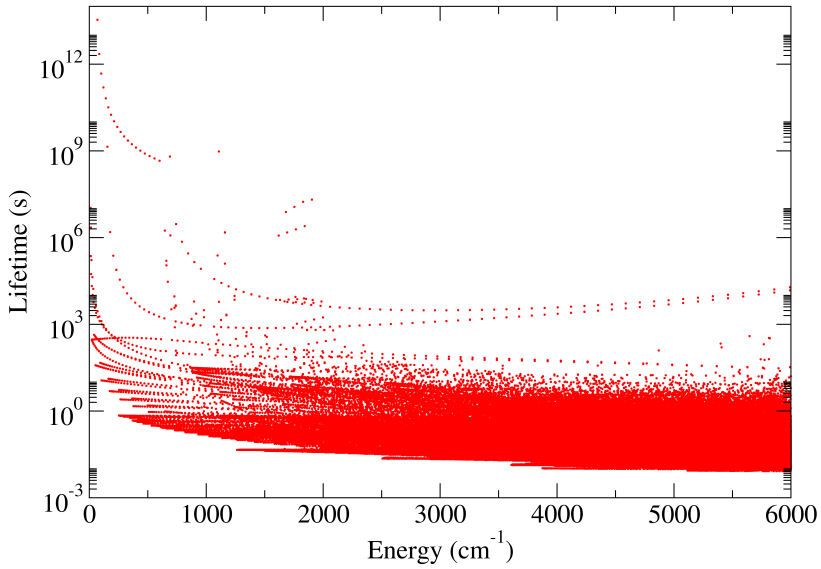

Figure 1. Radiative lifetimes computed (Tennyson et al. 2016a) for H_2O_2 states up to 6,000 cm^{-1}.

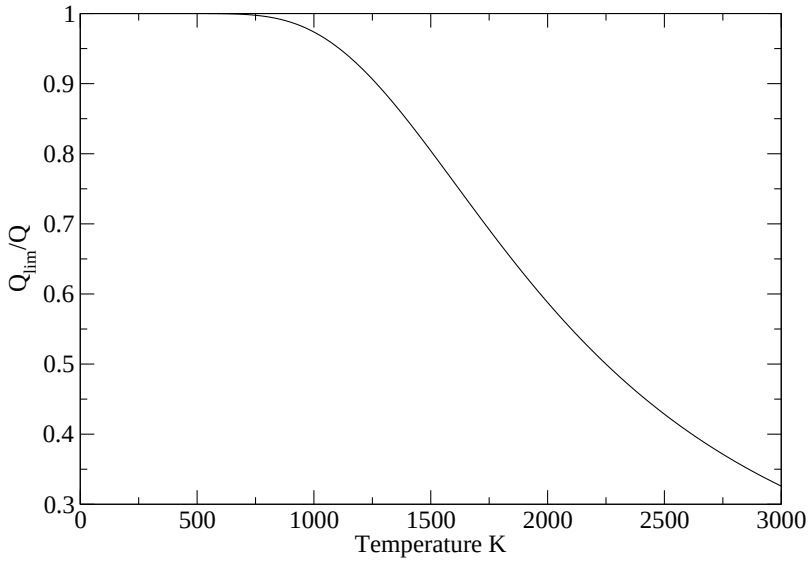

Figure 2. $Q_{\rm lim}/Q$ against temperature where $Q_{\rm limit}$ is the partition function computed using only energy levels below our lower state threshold of 6000 cm^{-1} and Q is our estimate of the full partition function.

data. Table 7 shows that for the limit available empirical band intensities we agree with most regions to $\leqslant$7.3% which is below the estimated experimental uncertainty of $\approx \pm$10%. Two discrepancies are with the v_6 band from Perrin et al. (1995) and the $\nu_2 + \nu_6$ band from Johnson et al. (2009). The former conflicts with other measurements due to Johnson et al. (2009) and Klee et al. (1999) where integrated absorption intensities were measured directly, whilst the band intensities of Perrin et al. (1995) were obtained by summing a synthetic spectrum of only 27 276 transitions. Our $\nu_2 + \nu_6$ band intensity is 33.78% weaker than the experimentally derived value. Johnson et al. (2009) suggests that the assignment of this band is $\nu_2 + \nu_6$

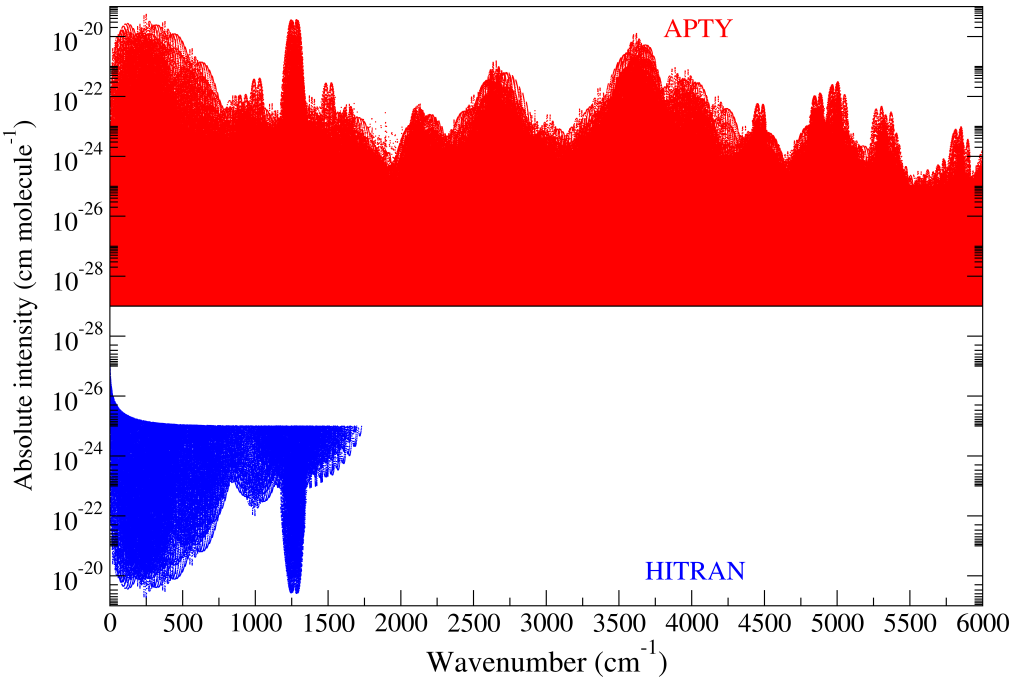

Figure 3. Overview of our synthetic spectrum at $T = 296$ K against HITRAN data (Rothman et al. 2013).

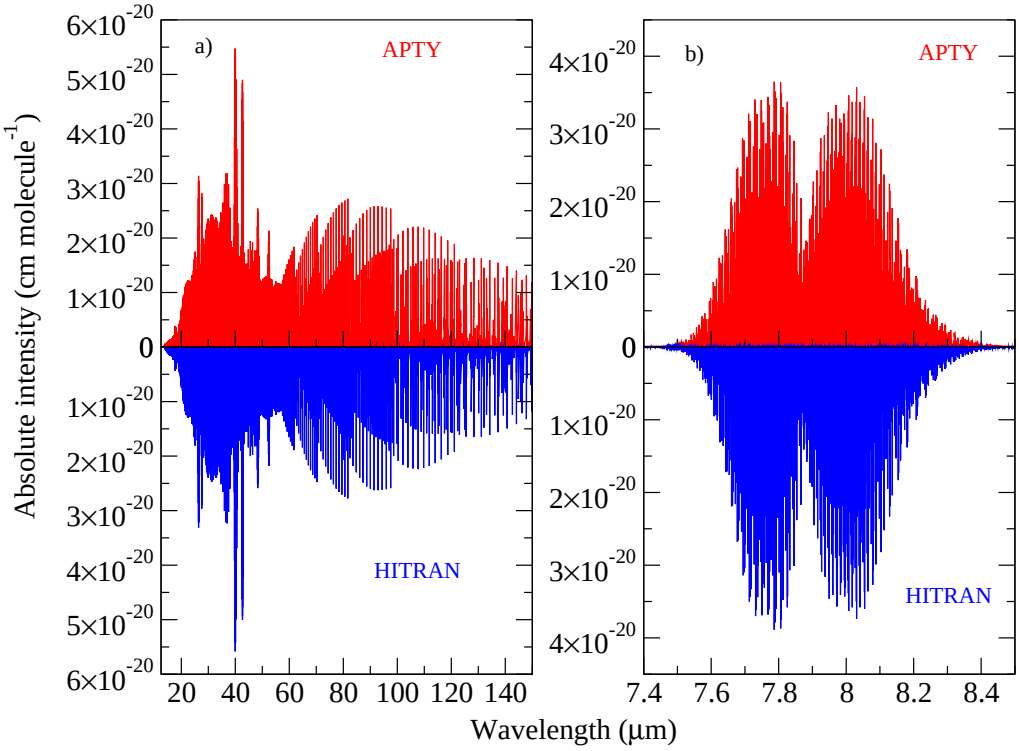

Figure 4. The fundamental bands compared to the HITRAN database (Rothman et al. 2013) at $T = 296$ K: (a) Torsional and (b) ν_6 bands.

Table 6. Comparisons of H_2O_2 partition functions as function of temperature for this work those used in HITRAN (Fischer et al. 2003).

T / K	APTY	HITRAN
75	895.506	894.866
150	2 815.866	2 811.187
255	7 360.598	7 336.856
300	10 126.961	10 087.090
500	31 246.17	30 990.11
1000	232 439.8	226 152.5
1500	1 031 673.6	993 983.8
3000	21 847 680	15 151 254

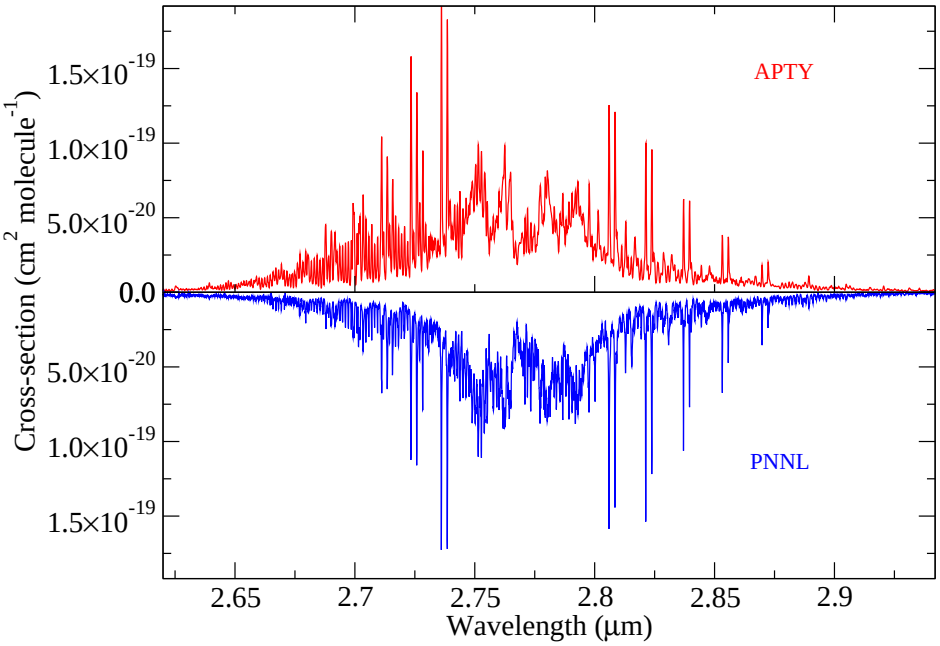

Figure 5. The ν_1 and ν_5 band region with APTY against PNNL-IR data at 323.15 K (Sharpe et al. 2004) with HWHM = 0.300 cm^{-1}

compared to the $\nu_2+\nu_3+\nu_4$ assignment by Giguere (1950). This is based on a Q-branch peak observed at 2,658.62 cm^{-1}. The assignments from APTY suggest that the peak observed is actually a convolution of Q-branches of the $(0,4) \rightarrow \nu_2 + (0,4)$, $(0,4) \rightarrow \nu_2 + (0,2) + \nu_6$, $(0,4) \rightarrow \nu_3 + (4,4)$, $(0,4) \rightarrow \nu_3 + (2,2)$, $(0,4) \rightarrow 2\nu_3 + (2,3)$ and $(0,4) \rightarrow \nu_3 + (2,2) + \nu_6$ transitions with an average separation between them at ≈0.02 cm^{-1}. Computing the band intensities of all of these bands in this region give an answer that agrees with value given by Johnson et al. (2009) to 3.97%.

The Kitt Peak Archive provides FTIR spectra of H_2O_2 covering the wavenumber region up to 6422 cm^{-1}, which is only partly assigned. Figure 7 (lower display) shows an uncalibrated spectrum of H_2O_2 in the 1.78 μm region (800628R0.002) recorded by R. H. Hunt in 1980, which covers the ν_1 and ν_5 fundamental bands of the hydrogen peroxide. To the best our knowledge these two bands have not been spectroscopically analysed. The upper display of this figures presents our absorption spectrum at 296 K simulated using the Doppler line profile. Our synthetic spectrum resembles all the main features of the experimental data. We would like to encourage a spectroscopic analysis of the Kitt Peak H_2O_2 spectra in the IR and near-IR regions currently not present in HITRAN. We believe that our theoretical line list with a capability of providing absolute intensities and quantum numbers can assist in the assignment of these spectra.

Figure 8 presents integrated absorption cross-sections computed using a Doppler profile (Hill et al. 2013) for a range of temperatures. The figure shows how the opacity changes with increasing temperature. We note the particularly dramatic effect raising the temperature has on the absorption by H_2O_2 in the 13.7 μm region. This smoothing in the overall spectra

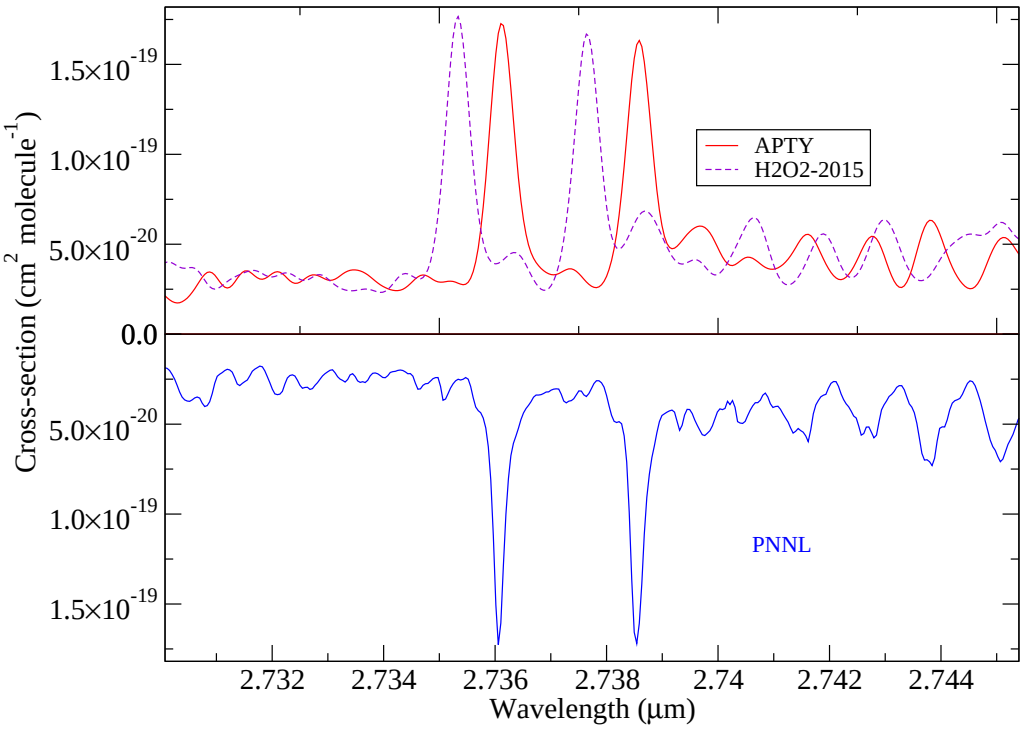

Figure 6. Cross-section comparison of peaks in the ν_1 and ν_5 band region with APTY (this work) and H2O2-2015 (Al-Refaie et al. 2015a) against PNNL-IR data at 323.15 K (Sharpe et al. 2004) with HWHM = 0.300 cm^{-1}

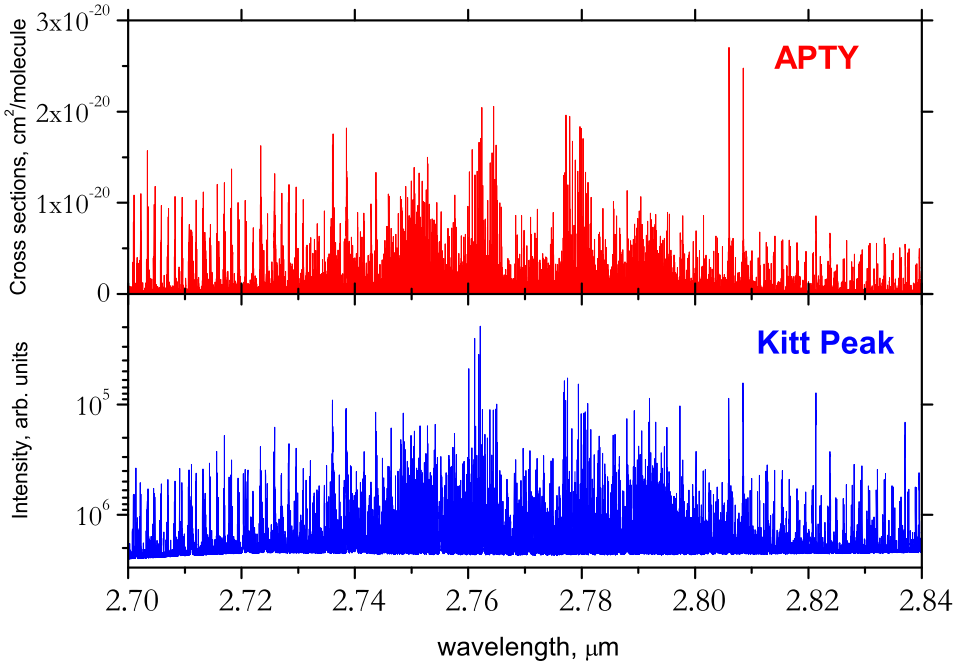

Figure 7. The 2.77 μm band of H_2O_2 at room temperature. Upper display: APTY cross-sections (296 K) generated using a Doppler profile; Lower display: an uncalibrated Kitt Peak spectrum of H_2O_2 (Archive Name is 800628R0.002, Date is 28/06/1980; Range is 1599.010271–6421.422198 cm^{-1}, Observer is Hunt; 1.77 m cell).

Table 7. Band intensities, in 10^{-17} cm^{-1}/(molecule cm^{-2}).

Band	Frequency range (cm^{-1})	Ref.	Obs	Calc	(O-C)/O (%)
Torsional	0–1,427	Perrin et al. (1996)	4.0400	3.7450	7.3
ν_3	750–1,100	Johnson et al. (2009)	0.0157	0.0165	-5.43
ν_6	1,135–1,393	Johnson et al. (2009)	1.7458	1.7651	-1.10
ν_6	1,170–1,380	Klee et al. (1999)	1.8500	1.7633	4.68
ν_6	1,170–1,380	Perrin et al. (1995)	1.0030	1.7633	-75.80
$\nu_2 + \nu_6$	2,300–2,900	Johnson et al. (2009)	0.0830	0.055	33.78
Multiple bands	2,300–2,900	Johnson et al. (2009)	0.0830	0.0797	3.97
ν_1,ν_5 region	3,300–3,800	Johnson et al. (2009)	0.8356	0.8724	-4.40

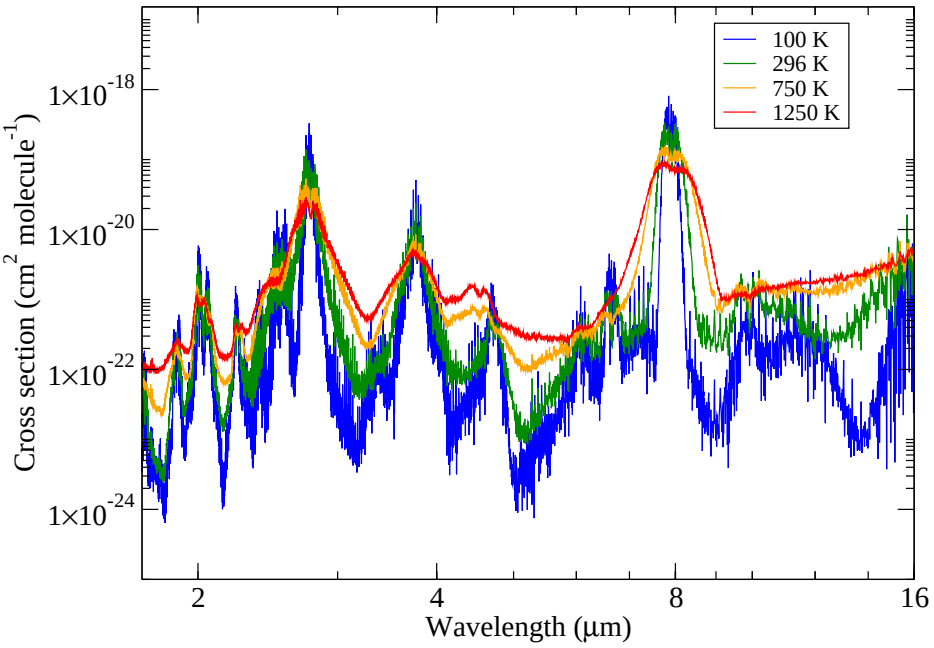

Figure 8. Cross-sections using a Doppler profile for the APTY line list as a function of temperature. The depth of the minima (windows) decreases monotonically with temperature.

can only be modelled if there is adequate coverage and population of rotationally and vibrationally excited states. We also note the strength of the OH stretch feature at about 2.75 μm; these features are absent from line databases such as HITRAN because of the absence of assigned spectra in this region. Hopefully APTY can be used to help analyse spectra in this region, as the BYTe NH_3 line list is being used to analyse ammonia spectra (Barton et al. 2015, 2016).

4 CONCLUSION

The frequency and Einstein-A coefficients of almost 20 billion transitions of hydrogen peroxide are computed. These transitions cover wavelengths longer than 1.6 μm and include all rotational excitations up to $J = 85$, making the line list applicable for temperatures up to 1250 K. The line list gives a room-temperature spectrum in excellent agreement with available experimental data and has good predictive ability for bands and line-positions not available experimentally. The new line list may be accessed via `www.exomol.com` or `http://cdsarc.u-strasbg.fr/viz-bin/qcat?J/MNRAS/`. The cross-sections of H_2O_2 can be also generated at `www.exomol.com` as described by Tennyson et al. (2016b).

5 ACKNOWLEDGEMENTS

This work was supported by the ERC under the Advanced Investigator Project 267219 and made use of the DiRAC@Darwin, DiRAC@COSMOS HPC cluster and Emerald CfI cluster. DiRAC is the UK HPC facility for particle physics, astrophysics and cosmology and is supported by STFC and BIS. The authors would like to acknowledge the work presented here made use of the EMERALD High Performance Computing facility provided via the Centre for Innovation (CfI). The CfI is formed from the universities of Bristol, Oxford, Southampton and UCL in partnership with STFC Rutherford Appleton Laboratory. We would also like to thank nVidia for supplying our group with a Tesla K40 GPU for usage in intensity and cross-section computation. AFA would also like to thank Dr. Faris N. Al-Refaie, Lamya Ali, Sarfraz Ahmed Aziz, and Rory and Annie Gleeson for their support.

REFERENCES

Al-Refaie A. F., Ovsyannikov R. I., Polyansky O. L., Yurchenko S. N., Tennyson J., 2015a, J. Mol. Spectrosc., 318, 84
Al-Refaie A. F., Tennyson J., Yurchenko S. N., 2016, Comput. Phys. Commun., (to be submitted)
Al-Refaie A. F., Yurchenko S. N., Yachmenev A., Tennyson J., 2015b, MNRAS, 448, 1704
Allen N. D. C., Abad G. G., Bernath P. F., Boone C. D., 2013, J. Quant. Spectrosc. Radiat. Transf., 115, 66
Anderson E. et al., 1999, LAPACK Users' Guide, 3rd edn. Society for Industrial and Applied Mathematics, Philadelphia, PA
Aoki S., Giuranna M., Kasaba Y., Nakagawa H., Sindoni G., Geminale A., Formisano V., 2015, Icarus, 245, 177
Bacelo D. E., Binning R. C., 2005, Intern. J. Quantum Chem., 105, 740
Bach R. D., Ayala P. Y., Schlegel H. B., 1996, J. Am. Chem. Soc., 118, 12758
Bartlett R. J., Musiał M., 2007, Rev. Mod. Phys., 79, 291
Barton E. J., Yurchenko S. N., Tennyson J., Béguier S., Campargue A., 2016, J. Mol. Spectrosc., (submitted)
Barton E. J., Yurchenko S. N., Tennyson J., Clausen S., Fateev A., 2015, J. Quant. Spectrosc. Radiat. Transf., 167, 126
Bergman P., Parise B., Liseau R., Larsson B., Olofsson H., Menten K. M., Güsten R., 2011, A&A, 531, L8
Blackford L. S. et al., 1997, ScaLAPACK Users' Guide. Society for Industrial and Applied Mathematics, Philadelphia, PA
Bowman J. M., Carter S., Huang X. C., 2003, Intern. J. Quantum Chem., 22, 533
Bunker P. R., Jensen P., 1998, Molecular Symmetry and Spectroscopy, 2nd edn. NRC Research Press, Ottawa
Camy-Peyret C., Flaud J.-M., Johns J. W. C., Noel M., 1992, J. Mol. Spectrosc., 155, 84
Carter S., Handy N. C., Bowman J. M., 2009, Mol. Phys., 107, 727
Carter S., Sharma A. R., Bowman J. M., 2011, J. Chem. Phys., 135, 014308
Chance K. V., Johnson D. G., Traub W. A., Jucks K. W., 1991, Geophys. Res. Lett., 18, 1003
Chen R. Q., Ma G. B., Guo H., 2001, J. Chem. Phys., 114, 4763
Clancy R. T., Sandor B. J., Moriarty-Schieven G. H., 2004, Icarus, 168, 116
Cooley J. W., 1961, Math. Comp., 15, 363
Davis D. D., 1974, Can. J. Chem., 52, 1405
Du F., Parise B., Bergman P., 2012, A&A, 538, A91
Encrenaz T. et al., 2004, Icarus, 170, 424
Encrenaz T., Greathouse T. K., Lefevre F., Atreya S. K., 2012, Planet Space Sci., 68, 3
Fischer J., Gamache R. R., Goldman A., Rothman L. S., Perrin A., 2003, J. Quant. Spectrosc. Radiat. Transf., 82, 401
Flaud J.-M., Camy-Peyret C., Johns J. W. C., Carli B., 1989, J. Chem. Phys., 91, 1504
Giguere P. A., 1950, J. Chem. Phys., 18, 88
Giguere P. A., Srinivasan T. K. K., 1974, J. Raman Spectrosc., 2, 125
Hand K. P., Brown M. E., 2013, ApJL, 766, L21
Hill C., Yurchenko S. N., Tennyson J., 2013, Icarus, 226, 1673
Hougen J. T., 1984, Can. J. Phys., 62, 1392
Johnson T. J., Sams R. L., Burton S. D., Blake T. A., 2009, Anal. Bioanal. Chem., 395, 377
Klee S., Winnewisser M., Perrin A., Flaud J.-M., 1999, J. Mol. Spectrosc., 195, 154
Koput J., Carter S., Handy N. C., 1998, J. Phys. Chem. A, 102, 6325
Kozin I. N., Law M. M., Tennyson J., Hutson J. M., 2004, Comput. Phys. Commun., 163, 117
Kuhn B., Rizzo T. R., Luckhaus D., Quack M., Suhm M. A., 1999, J. Chem. Phys., 111, 2565
Lin S. Y., Guo H., 2003, J. Chem. Phys., 119, 5867
Luckhaus D., 2000, J. Chem. Phys., 113, 1329
Małyszek P., Koput J., 2013, J. Comput. Chem., 34, 337
Mladenovic M., 2002, Spectra Chimica Acta A, 58, 809
Noumerov B. V., 1924, MNRAS, 84, 592

Olson W. B., Hunt R. H., Young B. W., Maki A. G., Brault J. W., 1988, J. Mol. Spectrosc., 127, 12
Perrin A., Flaud J.-M., Camy-Peyret C., Goldman A., Murcray F. J., Blatherwick R. D., 1990, J. Mol. Spectrosc., 142, 129
Perrin A. et al., 1996, J. Mol. Spectrosc., 176, 287
Perrin A., Valentin A., Flaud J. M., Camy-Peyret C., Schriver L., Schriver A., Arcas P., 1995, J. Mol. Spectrosc., 171, 358
Polyansky O. L., Kozin I. N., Maĺyszek P., Koput J., Tennyson J., Yurchenko S. N., 2013, J. Phys. Chem. A, 117, 7367
Rauhut G., Knizia G., Werner H.-J., 2009, J. Chem. Phys., 130, 054105
Rothman L. S. et al., 2013, J. Quant. Spectrosc. Radiat. Transf., 130, 4
Sharpe S. W., Johnson T. J., Sams R. L., Chu P. M., Rhoderick G. C., Johnson P. A., 2004, Appl. Spectrosc., 58, 1452
Sousa-Silva C., Al-Refaie A. F., Tennyson J., Yurchenko S. N., 2015, MNRAS, 446, 2337
Sousa-Silva C., Hesketh N., Yurchenko S. N., Hill C., Tennyson J., 2014, J. Quant. Spectrosc. Radiat. Transf., 142, 66
Tennyson J., Hill C., Yurchenko S. N., 2013, in AIP Conference Proceedings, Vol. 1545, 6^{th} international conference on atomic and molecular data and their applications ICAMDATA-2012, AIP, New York, pp. 186–195
Tennyson J., Hulme K., Naim O. K., Yurchenko S. N., 2016a, J. Phys. B: At. Mol. Opt. Phys., 49, 044002
Tennyson J., Yurchenko S. N., 2012, MNRAS, 425, 21
Tennyson J. et al., 2016b, J. Mol. Spectrosc.
Underwood D. S., Tennyson J., Yurchenko S. N., Clausen S., Fateev A., 2016, MNRAS, (submitted)
Underwood D. S., Yurchenko S. N., Tennyson J., Jensen P., 2014, J. Chem. Phys., 140, 244316
Vidler M., Tennyson J., 2000, J. Chem. Phys., 113, 9766
Yachmenev A., Yurchenko S. N., Jensen P., Thiel W., 2011, J. Chem. Phys., 134, 11
Yu H. G., Muckerman J. T., 2002, J. Mol. Spectrosc., 214, 11
Yurchenko S. N., Barber R. J., Tennyson J., 2011a, MNRAS, 413, 1828
Yurchenko S. N., Barber R. J., Tennyson J., Thiel W., Jensen P., 2011b, J. Mol. Spectrosc., 268, 123
Yurchenko S. N., Barber R. J., Yachmenev A., Thiel W., Jensen P., Tennyson J., 2009, J. Phys. Chem. A, 113, 11845
Yurchenko S. N., Carvajal M., Jensen P., Herregodts F., Huet T. R., 2003, Chem. Phys., 290, 59
Yurchenko S. N., Carvajal M., Jensen P., Lin H., Zheng J. J., Thiel W., 2005a, Mol. Phys., 103, 359
Yurchenko S. N., Tennyson J., 2014, MNRAS, 440, 1649
Yurchenko S. N., Thiel W., Carvajal M., Lin H., Jensen P., 2005b, Adv. Quant. Chem., 48, 209
Yurchenko S. N., Thiel W., Jensen P., 2007, J. Mol. Spectrosc., 245, 126
Zins E.-L., Krim L., 2014, RSC Adv., 4, 22172
Zumwalt L. A., Giguere P. A., 1941, J. Chem. Phys., 9, 458